Green's functions for Rossby waves

R.C. Kloosterziel[1] and L.R.M. Maas[2,3]

[1] School of Ocean & Earth Science & Technology, University of Hawaii, Honolulu, HI 96822, USA

[2] Institute for Marine & Atmospheric Research, Utrecht University, Princetonplein 5, 3584CC Utrecht, The Netherlands

[3] Royal Netherlands Institute for Sea Research, P.O. Box 59, 1790AB Texel, The Netherlands

(Received ?; revised ?; accepted ?. - To be entered by editorial office)

Compact solutions are presented for planetary, non-divergent, barotropic Rossby waves generated by (a) an impulsive point-source and (b) a sustained point-source of curl of wind-stress. Previously, only cumbersome integral expressions were known, rendering them practically useless. Our simple expressions allow for immediate numerical visualization/animation and further mathematical analysis.

1. Introduction

Non-divergent waves in a two-dimensional fluid layer on a rotating sphere, restored solely by Coriolis forces due to vorticity conservation, are present as second-class waves in Laplace's equations and were studied by Margules (1893) and Hough (1898). Their nature was clarified when Rossby & collaborators (1939) derived a simplified version of the barotropic vorticity equation on a mid-latitude tangent plane (β-plane). They eliminated the first-class, gravity waves by assuming a rigid lid. Thus they considered non-divergent flow in a fluid layer in which vorticity changes in time due to advection of variations in background, planetary vorticity. Linear, free-wave solutions of this equation display strictly westward phase propagation, but west or eastward energy propagation for long and short waves, respectively. In recognition of the value of this clarification, these waves are nowadays called Rossby waves. They are forced by curl of the wind stress and the barotropic, non-divergent linear motions are governed by

$$\partial_t q + \beta v = \mathrm{curl}\, \boldsymbol{\tau}. \tag{1.1}$$

The relative vorticity $q = \partial_x v - \partial_y u$ is created by south-north advection of planetary vorticity and by $\boldsymbol{\tau} = \{\tau_x, \tau_y\}$ the wind-stress vector (see e.g. Veronis (1958); Pedlosky (1987)). As usual, t is time, x longitude, y latitude and βv is the advection of planetary vorticity by the latitudinal (south-north) velocity component v.

Introducing a streamfunction ψ, so that the velocity components are $u = -\partial_y \psi, v = \partial_x \psi$ and $q = \nabla^2 \psi$, equation (1.1) becomes $\partial_t \nabla^2 \psi + \beta \partial_x \psi = \mathrm{curl}\, \boldsymbol{\tau}$ with $\nabla^2 = (\partial_x^2 + \partial_y^2)$. In this study, the Green's function G_δ for an 'impulsive point source' and G_{H} for a 'switch-on point source' are defined as solutions of

$$(a) \quad \mathcal{L} G_\delta = \delta(t)\delta(x)\delta(y), \quad (b) \quad \mathcal{L} G_{\mathrm{H}} = \mathrm{H}(t)\delta(x)\delta(y), \qquad \mathcal{L} = \partial_t \nabla^2 + \beta \partial_x. \tag{1.2}$$

$\mathcal{L}$ is the Rossby wave operator, δ the usual Dirac delta-function and H the Heaviside unit stepfunction and by definition $\delta(t) \equiv \mathrm{dH}(t)/\mathrm{d}t$. In this paper we shall show that

$$G_\delta = \frac{\mathrm{H}(t)}{4} [J_0(z_+) Y_0(z_-) + J_0(z_-) Y_0(z_+)], \tag{1.3}$$

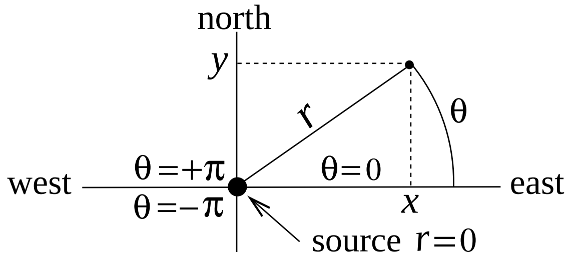

FIGURE 1. The Cartesian $\{x, y\}$ and cylindrical $\{r, \theta\}$ coordinate systems. The forcing location for G_δ and G_{H} at $r = 0$ is indicated by ●. 'East' is defined by $\theta = 0$, 'west' by $\theta = \pm\pi$, 'north' by $\theta = \pi/2$, r is the distance from the source and $x = r\cos\theta, y = r\sin\theta$.

$$G_{\mathrm{H}} = \frac{t\mathrm{H}(t)}{2(z_+^2 - z_-^2)}\left[z_+J_1(z_+)Y_0(z_-) - z_-J_1(z_-)Y_0(z_+) \right. \\ \left. + z_+J_0(z_-)Y_1(z_+) - z_-J_0(z_+)Y_1(z_-)\right]. \tag{1.4}$$

In (1.3) and (1.4) J_n, Y_n are nth-order Bessel functions of the first and second kind, respectively, with complex conjugate arguments

$$z_+ = \sqrt{\beta tr}\mathrm{e}^{+\mathrm{i}\theta/2}, \quad z_- = \sqrt{\beta tr}\mathrm{e}^{-\mathrm{i}\theta/2} \quad \text{or} \quad z_\pm = \sqrt{\beta t(x \pm \mathrm{i}y)}. \tag{1.5}$$

The usual cylindrical coordinate system $\{r, \theta\}$ is employed with the origin at the forcing location (see figure 1). The prefactor $\mathrm{H}(t)$ in (1.3) and (1.4) enforces 'causality', i.e. $G_{\delta,\mathrm{H}} = 0$ for $t < 0$. Since efficient algorithms for Bessel functions exist, the compact expressions in (1.3) and (1.4) allow for a quick evaluation: with a few lines of code in little time a movie can be created visualizing the temporal and spatial evolutions.

Typically in finding Green's functions and such as solutions of linear partial differential equations like (1.2), well-established theory for Laplace and/or Fourier-transforms is used in combination with theory of differential equations. Various integral representations for G_δ and G_{H} that have been derived in such a manner are briefly reviewed in §2. They also reveal a relation between G_δ and G_{H}: not only is $\partial_t G_{\mathrm{H}} = G_\delta$, as expected, but once G_δ is known G_{H} follows by differentiation of G_δ with respect to the polar angle θ. Precise numerical evaluation of the integral representation is cumbersome, but for locations exactly east ($\theta = 0$) and west ($\theta = \pm\pi$) of the source they can be evaluated exactly. Our new expressions for G_δ and G_{H} provide a complete 'picture' at any angle θ with the east-west axis.

The compact formula (1.3) for G_δ was discovered by recognizing that a particular integral representation of G_δ is essentially an integral of the kind studied by Dixon & Ferrar (1933). Differentiation of (1.3) then quickly yielded G_{H} given by (1.4). This is discussed in §3 where, for completeness' sake, we also show that the Green's functions given by (1.3) and (1.4) indeed solve (1.2). In §4 we provide illustrative graphs of G_δ and G_{H} and derive simple approximations which presume large arguments $|z_\pm|$ or $\sqrt{\beta tr} \gg 1$. Also in §4 the associated wave-energy density distributions are considered. In §5 we discuss the ramifications of this study and in particular we draw attention to results that indicate that parabolic coordinates $\zeta = \sqrt{r + x}$, $\eta = \sqrt{r - x}$ appear to be a natural choice when studying non-divergent Rossby waves.

2. Integral representations and relations between G_δ and G_H

Veronis (1958) showed that

$$G_\delta = -\frac{\mathrm{H}(t)}{\pi}\int_0^\infty \frac{J_0\left(2\sqrt{\beta tr(\eta^2+\cos^2\frac{1}{2}\theta)}\right)}{\sqrt{\eta^2+1}}\mathrm{d}\eta, \tag{2.1}$$

correcting for a typographical error. He called the point-size burst of wind-stress-curl a 'tweak' and derived (2.1) through the use of a Laplace transform in time of (1.2*a*) which reduced the problem to solving a second-order partial differential equation (in variables x, y). With the solution at hand, (2.1) followed from the inverse Laplace transform. Longuet-Higgins (1965) also found (2.1), but through a triple Fourier-transform. Much later, Kamenkovich (1989) established that

$$G_\mathrm{H} = -\frac{\mathrm{H}(t)}{\pi}\sqrt{\frac{t}{\beta r}}\int_0^\infty \frac{J_1\left(2\sqrt{\beta tr(\eta^2+\cos^2\frac{1}{2}\theta)}\right)}{\sqrt{\eta^2+1}\sqrt{\eta^2+\cos^2\frac{1}{2}\theta}}\mathrm{d}\eta, \tag{2.2}$$

using a Laplace transform of (1.2*b*) with respect to time. Both infinite integrals defining $G_{\delta,\mathrm{H}}$ are difficult to evaluate numerically due to the oscillatory behavior of J_0, J_1 for increasing η. However, computationally more efficient integral expressions for G_δ have been found by Llewellyn-Smith (1997).

The integral representation (2.1) for G_δ reduces on the east-west axis to

$$\theta = 0 \text{ (east)}: \qquad G_\delta = \frac{J_0(\sqrt{\beta tr})Y_0(\sqrt{\beta tr})}{2}, \tag{2.3a}$$

$$\theta = \pm\pi \text{ (west)}: \qquad G_\delta = -\frac{I_0(\sqrt{\beta tr})K_0(\sqrt{\beta tr})}{\pi}, \tag{2.3b}$$

with I_n, K_n the nth-order modified Bessel functions of the first and second kind, respectively. For convenience we have dropped the 'causality switch' $\mathrm{H}(t)$. The limiting case $\theta = \pm\pi$ (2.3*b*) was first noted, apart from a missing minus sign, by Longuet-Higgins (1965) but for $\theta = 0$ he erred. The correct limit $\theta = 0$ in (2.3*a*) was given by Llewellyn-Smith (1997). Kamenkovich (1989) recognized with the integral representation (2.2) that G_H reduces on the east-west axis to

$$\theta = 0 \text{ (east)}: \qquad G_\mathrm{H} = \frac{t}{2}\left[J_0(\sqrt{\beta tr})Y_0(\sqrt{\beta tr}) + J_1(\sqrt{\beta tr})Y_1(\sqrt{\beta tr})\right], \tag{2.4a}$$

$$\theta = \pm\pi \text{ (west)}: \qquad G_\mathrm{H} = -\frac{t}{\pi}\left[I_0(\sqrt{\beta tr})K_0(\sqrt{\beta tr}) + I_1(\sqrt{\beta tr})K_1(\sqrt{\beta tr})\right]. \tag{2.4b}$$

Simpler integral expressions

$$G_\delta = -\frac{1}{4\pi}\int_{-\infty}^{+\infty} J_0\left(\sqrt{2\beta tr(\cosh\nu+\cos\theta)}\right)\mathrm{d}\nu, \tag{2.5a}$$

$$G_\mathrm{H} = -\frac{t}{2\pi}\int_{-\infty}^{+\infty} \frac{J_1\left(\sqrt{2\beta tr(\cosh\nu+\cos\theta)}\right)}{\sqrt{2\beta tr(\cosh\nu+\cos\theta)}}\mathrm{d}\nu, \tag{2.5b}$$

follow from (2.1) and (2.2) through substitution of $\eta = \sinh\frac{1}{2}\nu$. Note that G_δ is a function of the similarity variables βtx, βty or $G_\delta = F(\beta tr, \theta)$ while G_H is of the form $tF(\beta tr, \theta)$.

To proceed, observe how on the east side ($\theta = 0$), integral expression (2.5*a*) for G_δ

simplifies to

$$G_\delta = -\frac{1}{4\pi}\int_{-\infty}^{+\infty} J_0\left(2\sqrt{\beta tr}\cosh\tfrac{1}{2}\nu\right)\mathrm{d}\nu = -\frac{1}{2\pi^2}\iint_{-\infty}^{+\infty}\sin\left(2\sqrt{\beta tr}\cosh\nu'\cosh\mu\right)\mathrm{d}\nu'\mathrm{d}\mu,$$

where we use $\nu' = \frac{1}{2}\nu$, and the first of the integral expressions for the Bessel functions

$$J_0(x) = \frac{1}{\pi}\int_{-\infty}^{+\infty}\sin(x\cosh\mu)\mathrm{d}\mu, \quad Y_0(x) = -\frac{1}{\pi}\int_{-\infty}^{+\infty}\cos(x\cosh\mu)\mathrm{d}\mu. \qquad (2.6a,b)$$

Setting $m = \mu + \nu'$, $n = \mu - \nu'$, we rotate integration variables μ, ν' over $\pi/4$, yielding

$$G_\delta = -\frac{1}{4\pi^2}\int_{-\infty}^{+\infty}\int_{-\infty}^{+\infty}\sin\left(\sqrt{\beta tr}[\cosh m + \cosh n]\right)\mathrm{d}m\mathrm{d}n.$$

Using the trigonometric identity $\sin(a+b) = \sin a\cos b + \sin b\cos a$, this integral is separable and leads with the Bessel identities (2.6a,b) to (2.3a), i.e.

$$\begin{aligned} G_\delta = -\frac{1}{4\pi^2}\Bigg(&\int_{-\infty}^{+\infty}\sin\left(\sqrt{\beta tr}\cosh m\right)\mathrm{d}m\int_{-\infty}^{+\infty}\cos\left(\sqrt{\beta tr}\cosh n\right)\mathrm{d}n \\ &+\int_{-\infty}^{+\infty}\cos\left(\sqrt{\beta tr}\cosh m\right)\mathrm{d}m\int_{-\infty}^{+\infty}\sin\left(\sqrt{\beta tr}\cosh n\right)\mathrm{d}n\Bigg) = \frac{J_0(\rho)Y_0(\rho)}{2}, \end{aligned} \qquad (2.7)$$

with $\rho \equiv \sqrt{\beta tr}$. A similar derivation can be used to obtain the established result (2.3b) on the west-axis ($\theta = \pm\pi$).

Since G_{H} describes the response to sustained forcing represented by the Heaviside function $\mathrm{H}(t)$ and G_δ to impulsive forcing represented by $\delta(t)$, one expects $G_\delta = \partial G_{\mathrm{H}}/\partial t$. The integral representations for G_δ and G_{H} confirm this. For example, in (2.5b)

$$G_{\mathrm{H}} = \frac{1}{2\pi}\int_{-\infty}^{+\infty}\frac{tJ_0'(z)}{z}\mathrm{d}\nu, \qquad z \equiv \sqrt{2\beta tr(\cosh\nu + \cos\theta)}, \qquad (2.8)$$

where we used the fact that $J_1 = -J_0'$ (a prime indicates differentiation). Since $\partial z/\partial t = z/2t$, it follows that

$$\begin{aligned} \frac{\partial G_{\mathrm{H}}}{\partial t} &= \frac{1}{2\pi}\left[\int\frac{J_0'(z)}{z}\mathrm{d}\nu + \int t\left(\frac{J_0''(z)}{z}\frac{z}{2t} - \frac{J_0'(z)}{z^2}\frac{z}{2t}\right)\mathrm{d}\nu\right] \\ &= \frac{1}{2\pi}\left[\int\frac{1}{2}\left(\frac{J_0'(z)}{z} + J_0''(z)\right)\mathrm{d}\nu\right] = -\frac{1}{4\pi}\int J_0(z)\mathrm{d}\nu = (2.5a) = G_\delta \end{aligned} \qquad (2.9)$$

because J_0 solves the Bessel equation $z^2J_0'' + zJ_0' + z^2J_0 = 0$.

Another relation exists between G_δ and G_{H}: In (2.5b)

$$\frac{tJ_1(z)}{z} = \frac{1}{\beta r\sin\theta}\frac{\partial J_0(z)}{\partial\theta}. \qquad (2.10)$$

Comparison with (2.5a) shows that

$$G_{\mathrm{H}} = \frac{2}{\beta r\sin\theta}\frac{\partial G_\delta}{\partial\theta} \quad \text{and} \quad \left(\frac{\partial^2}{\partial t\partial\theta} - \tfrac{1}{2}\beta r\sin\theta\right)G_{\mathrm{H}} = 0 \qquad (2.11a,b)$$

because $G_\delta = \partial_t G_{\mathrm{H}}$. Time differentiation shows that therefore G_δ also satisfies (2.11b).

3. Closed-form expressions for G_δ and G_{H}

In view of the definition of $z_\pm$ in (1.5), the integral representation (2.5*a*) equals

$$G_\delta = -\frac{1}{4\pi}\int_{-\infty}^{+\infty} J_0\left(\sqrt{z_+^2 + z_-^2 + 2z_+z_-\cosh\nu}\right)\mathrm{d}\nu. \tag{3.1}$$

This observation led us to the expression (1.3) for G_δ as follows. Dixon & Ferrar (1933) considered products of modified Bessel functions of the second kind $K_{\nu,\mu}$ and showed that such products can be reduced to a single integral involving $K_{\nu+\mu}$, provided certain conditions are met. For the purpose of this paper it suffices to point out that one of their results implies that for real $x, y > 0$

$$K_0(\mathrm{i}x)K_0(\mathrm{i}y) = \int_{-\infty}^{+\infty} K_0(\mathrm{i}\lambda)\mathrm{d}t', \qquad \lambda = \sqrt{x^2 + y^2 + 2xy\cosh 2t'} \tag{3.2}$$

(Dixon & Ferrar (1933), formula 3.32). Connection formulas tell us further that

$$K_0(z) = -\tfrac{1}{2}\pi\mathrm{i}H_0^{(2)}(-\mathrm{i}z), \quad -\tfrac{1}{2}\pi \leqslant \mathrm{ph}\, z \leqslant \pi, \tag{3.3}$$

with the Hankel function $H_0^{(2)} = J_0 - \mathrm{i}Y_0$ (see the NIST *Handbook of Mathematical functions*, Olver *et al.* (2010), formula 10.27.8). Specifically this means $K_0(\mathrm{i}x) = -\frac{1}{2}\pi\mathrm{i}H_0^{(2)}(x)$ and likewise for y. Therefore with (3.2) it follows that

$$\begin{aligned}\int_{-\infty}^{+\infty}[J_0(\lambda) - \mathrm{i}Y_0(\lambda)]\mathrm{d}t' &= \int_{-\infty}^{+\infty} H_0^{(2)}(\lambda)\mathrm{d}t' = -\frac{\pi\mathrm{i}}{2}H_0^{(2)}(x)H_0^{(2)}(y)\\ &= -\frac{\pi}{2}[J_0(x)Y_0(y) + J_0(y)Y_0(x)] - \frac{\pi\mathrm{i}}{2}[J_0(x)J_0(y) - Y_0(x)Y_0(y)]\end{aligned} \tag{3.4}$$

(for the more general case involving $H_\nu^{(2)}(x)H_\mu^{(2)}(y)$ see formula 17.4.2 (76) in Erdélyi (1953) and for related results Magnus *et al.* (1966), page 93, which contains a typographical error though). Equating real parts in (3.4) leads to the product $J_0(x)Y_0(y) + J_0(y)Y_0(x)$ expressed as an integral over $J_0(\lambda)$. Comparison with the integral expression (3.1) shows that the closed-form expression (1.3) would follow if we could simply substitute $x = z_+$, $y = z_-$ in (3.4) after setting $\nu = 2t'$ in (3.1). Thus we surmised that G_δ given in (1.3) is the solution of (1.2a). This 'educated guess' proved to be correct by direct verification (see below).

However, S.G. Llewellyn-Smith (University of California, San Diego) pointed out during the revision process of this manuscript that the results of Dixon & Ferrar (1933) in fact imply that (3.1) equals (1.3) when the principle of analytic continuation is invoked. Again tailored specifically to our needs here, Dixon & Ferrar (1933) state that for complex variables Z, z with positive real parts (absolute phase $< \pi/2$)

$$K_0(Z)K_0(z) = \int_{-\infty}^{+\infty} K_0(\sqrt{Z^2 + z^2 + 2Zz\cosh 2t'})\mathrm{d}t', \quad |\mathrm{ph}\, Z,\, z| < \frac{\pi}{2}. \tag{3.5}$$

The Bessel functions are analytic when a branch cut is made on the negative real axis, i.e. for $\mathbb{C}\backslash(-\infty, 0]$. If we exclude the west-axis ($\theta = \pm\pi$), equation (3.5) is valid when $Z = z_+, z = z_-$ is substituted (for $\theta = \pi$ we have $z_\pm = \pm\mathrm{i}\sqrt{\beta tr}$ and for $\theta = -\pi$ we have $z_\pm = \mp\mathrm{i}\sqrt{\beta tr}$ according to (1.5)). Both variables lie in the open right-half of the complex plane and if rotated anti-clockwise by an angle ϕ they become $z'_\pm = \mathrm{e}^{\mathrm{i}\phi}z_\pm$. For $\phi = \pi/2$ the rotated $z'_\pm = \mathrm{i}z_\pm$ have been moved to the upper half of the complex plane without crossing the negative real axis. Therefore the left-hand side of (3.5) remains analytic. The argument of K_0 in the integral becomes under this rotation

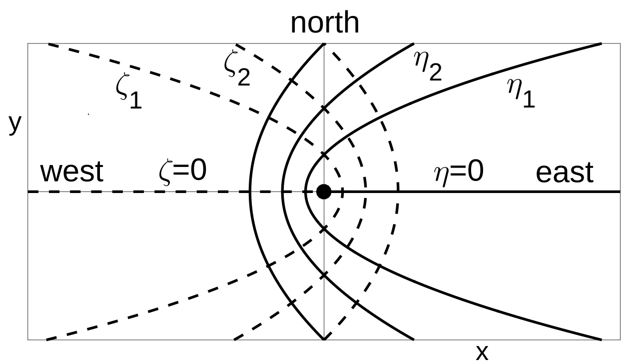

FIGURE 2. The parabolic coordinate system $\{\zeta, \eta\}$ with $\zeta = \sqrt{r+x}$, $\eta = \sqrt{r-x}$ defined in (3.8). The entire western axis $x < 0$, $y = 0$ coincides with $\zeta = 0$, the eastern axis $x > 0$, $y = 0$ with $\eta = 0$. The origin $\zeta = \eta = 0$ indicated by ● is the forcing location as in figure 1.

simply $e^{i\phi}\sqrt{2\beta t r(\cos\theta + \cosh 2t')}$. Thus, if the west-axis is excluded from consideration, as ϕ is increased towards $\pi/2$ the argument never crosses the branch cut of K_0 and the integrand and the integral on the right-hand side of (3.5) remain analytic. By analytic continuation we therefore find that

$$K_0(iz_+)K_0(iz_-) = \int_{-\infty}^{+\infty} K_0\left(i\sqrt{z_+^2 + z_-^2 + 2z_+z_-\cosh 2t'}\right) dt'. \qquad (3.6)$$

The conditions for (3.3) to be valid are met and we can, just as shown above for real x, y, equate the real parts on the left and right in (3.6). This establishes that the integral representation (3.1) equals the closed-form expression (1.3) for G_δ. Despite this compelling argument, we nonetheless verify the validity of (1.3) below and show how G_{H} (1.4) was derived.

3.1. *Validation of G_δ*

In order to verify that G_δ (1.3) is correct, it is expedient to write the complex conjugate variables $z_\pm$ introduced in (1.5) as

$$z_+ = a z_\star, \quad z_- = a\bar{z}_\star, \quad a = \sqrt{\frac{\beta t}{2}}, \quad z_\star \equiv \zeta + i\eta, \quad \bar{z}_\star \equiv \zeta - i\eta \qquad (3.7)$$

with parabolic coordinates

$$\zeta = \sqrt{r(1+\cos\theta)} = \sqrt{r+x}, \quad \eta = \sqrt{r(1-\cos\theta)} = \sqrt{r-x}. \qquad (3.8)$$

Lines of constant ζ are parabolas that open towards the west ($x < 0$) and constant η parabolas that open towards the east ($x > 0$) as sketched in figure 2. The Laplace operator in these coordinates is well-known (see Moon & Spencer (1961)) while $\partial/\partial x$ is easily calculated with the chain rule. They are

$$\nabla^2 = \frac{1}{\zeta^2+\eta^2}\left[\frac{\partial^2}{\partial\zeta^2} + \frac{\partial^2}{\partial\eta^2}\right], \qquad \frac{\partial}{\partial x} = \frac{1}{2r}\left[\zeta\frac{\partial}{\partial\zeta} - \eta\frac{\partial}{\partial\eta}\right]. \qquad (3.9)$$

But $2r = \zeta^2 + \eta^2$ and the Rossby wave operator becomes

$$\mathcal{L} = \frac{1}{\zeta^2+\eta^2}\left\{\frac{\partial}{\partial t}\left(\frac{\partial^2}{\partial\zeta^2}+\frac{\partial^2}{\partial\eta^2}\right)+\beta\left(\zeta\frac{\partial}{\partial\zeta}-\eta\frac{\partial}{\partial\eta}\right)\right\}. \tag{3.10}$$

With a few elementary manipulations one finds next that

$$\mathcal{L} = \frac{1}{z_\star\bar{z}_\star}\left\{4\frac{\partial}{\partial t}\left(\frac{\partial^2}{\partial z_\star\partial\bar{z}_\star}\right)+\beta\left(\bar{z}_\star\frac{\partial}{\partial z_\star}+z_\star\frac{\partial}{\partial\bar{z}_\star}\right)\right\}. \tag{3.11}$$

With (3.11) it follows, after collecting terms, that

$$\begin{aligned}\mathcal{L}\, J_0(z_+)Y_0(z_-) = \frac{\beta}{z_\star\bar{z}_\star}&\{J_0'(z_+)\left[z_-Y_0''(z_-)+Y_0'(z_-)+z_-Y_0(z_-)\right]\\ &+Y_0'(z_-)\left[z_+J_0''(z_+)+J_0'(z_+)+z_+J_0(z_+)\right]\}=0\end{aligned} \tag{3.12}$$

because J_0, Y_0 satisfy the Bessel equation

$$z^2\mathcal{J}_0''+z\mathcal{J}_0'+z^2\mathcal{J}_0=0. \tag{3.13}$$

Clearly also $\mathcal{L}J_0(z_-)Y_0(z_+)=0$ and away from $z_\star\bar{z}_\star=2r=0$ for $t>0$ indeed $\mathcal{L}G_\delta=0$.

The $\delta(t)\delta(x)\delta(y)$ singularity in (1.2*a*) has to come from the term $\partial_t\nabla^2G_\delta$. The $\delta(t)$ behavior must be associated with the time-derivative of $\mathrm{H}(t)$ which multiplies $J_0(z_+)Y_0(z_-)+J_0(z_-)Y_0(z_+)$ in (1.3). Replacing $\delta(x)\delta(y)$ on the right-hand side of (1.2*a*) by $\delta(r)/(2\pi r)$, for small r the Green's function must therefore behave as $G_\delta\approx\mathrm{H}(t)\ln r/2\pi$. That this is true is seen as follows: Since for small z

$$z\to 0:\quad J_0(z)\approx 1,\quad Y_0(z)\approx(2/\pi)\ln z, \tag{3.14}$$

near the origin

$$r\downarrow 0:\ G_\delta\approx\frac{\mathrm{H}(t)}{4}\left[\frac{2}{\pi}\ln z_-+\frac{2}{\pi}\ln z_+\right]=\frac{\mathrm{H}(t)}{2\pi}\ln\beta tr=\frac{\mathrm{H}(t)}{2\pi}\left[\ln r+\ln\beta t\right] \tag{3.15}$$

because, according to (1.5), $z_\pm=\sqrt{\beta tr\mathrm{e}^{\pm\mathrm{i}\theta}}$. The part that only depends on time t plays no role in getting $\delta(t)\delta(x)\delta(y)$ from $\partial_t\nabla^2G$ and therefore (1.3) has the correct behavior near the origin. Finally, on the x-axis in the limit $\theta\to 0$ (east) we have $z_+=z_-=\sqrt{\beta tr}$ and it is seen with (1.3) that for $t>0$ (2.3*a*) is recovered. For $\theta\to\pi$ (west) we have $z_\pm=\pm\mathrm{i}\sqrt{\beta tr}$ and connection formulas are needed. They imply that $J_0(z_\pm)\to I_0(\sqrt{\beta tr})$ and that

$$\theta\to\pi:\quad Y_0(z_+)\to\mathrm{i}I_0(\sqrt{\beta tr})-\frac{2}{\pi}K_0(\sqrt{\beta tr}),\quad Y_0(z_-)\to-\mathrm{i}I_0(\cdots)-\frac{2}{\pi}K_0(\cdots) \tag{3.16}$$

(see the NIST *Handbook of Mathematical functions* (Olver *et al.* (2010)), formulas 10.27.6 and 10.27.11). Substituting this in (1.3) we find (2.3*b*). The same result is found in the limit $\theta=-\pi$. This proves that G_δ is correct.

3.2. *Derivation and validation of* G_{H}

The integral representations showed that G_{H} can be obtained through differentiation of G_δ according to (2.11a). With the $\{z_\star,\bar{z}_\star\}$ variables we find that (2.11a) becomes

$$G_{\mathrm{H}}=-\frac{4}{\beta(z_\star^2-\bar{z}_\star^2)}\left[z_\star\frac{\partial}{\partial z_\star}-\bar{z}_\star\frac{\partial}{\partial\bar{z}_\star}\right]G_\delta. \tag{3.17}$$

Substitution of $G_\delta=\frac{1}{4}\left[J_0(az_\star)Y_0(a\bar{z}_\star)+c.c.\right]$ results in the expression (1.4) for G_{H} with the definition of $z_\pm$ given in (3.7) and use of the fact that $J_0'=-J_1$ and $Y_0'=-Y_1$. Also the integral representations implied $\partial_t G_{\mathrm{H}} = G_\delta$. According to (3.17) this is true if

$$G_\delta = -\frac{2t}{z_+^2 - z_-^2}\left[z_+\frac{\partial}{\partial z_+} - z_-\frac{\partial}{\partial z_-}\right]\frac{\partial G_\delta}{\partial t}, \tag{3.18}$$

having restored $z_\pm$ on the right-hand side. We find, for example, that

$$\frac{\partial J_0(z_+)Y_0(z_-)}{\partial t} = \left[z_+J_0'(z_+)Y_0(z_-) + z_-J_0(z_+)Y_0'(z_-)\right]/2t \qquad \text{and}$$

$$\left[z_+\frac{\partial}{\partial z_+} - z_-\frac{\partial}{\partial z_-}\right]\frac{\partial J_0(z_+)Y_0(z_-)}{\partial t} = -\frac{z_+^2 - z_-^2}{2t}J_0(z_+)Y_0(z_-)$$

after use of the Bessel equation (3.13). It quickly follows with (1.3) for G_δ that indeed $\partial_t G_{\mathrm{H}} = G_\delta$. Moreover, since we know $\mathcal{L}G_\delta = 0$ for $r \neq 0$ and therefore $\partial_t\mathcal{L}G_{\mathrm{H}} = 0$, it follows that $\mathcal{L}G_{\mathrm{H}} = 0$ ($\mathcal{L}G_{\mathrm{H}} = f(x,y) \neq 0$ can be ruled out).

The singularity at the origin has to come from $\partial_t\nabla^2 G_{\mathrm{H}}$ in (1.2b) and the factor $\mathrm{H}(t)$ on the right-hand side must be due to a time-derivative of $t\mathrm{H}(t)$. Therefore for small r the Green's function must behave as $G_{\mathrm{H}} \approx t\mathrm{H}(t)\ln r/2\pi$. That this is true follows with (3.14) for J_0, Y_0 and the fact that

$$z \to 0: \quad J_1(z) \sim z/2, \quad Y_1(z) \sim -2/(\pi z) + (z/\pi)\ln z. \tag{3.19}$$

When put in (1.4), we find that for small r

$$r \downarrow 0: \; G_{\mathrm{H}} \approx \frac{t\mathrm{H}(t)}{2\pi}[\ln r + \ln \beta t]. \tag{3.20}$$

Again the part that only depends on t is irrelevant, and G_{H} has the correct singularity.

Finally, it is easily verified with the Bessel equation (3.13) that ∂_t(2.4a)=(2.3a). Also one finds ∂_t(2.4b)=(2.3b) through use of $I_0' = I_1$, $K_0' = -K_1$ and the fact that $I_0(z)$ satisfies $z^2\mathcal{I}_0'' + z\mathcal{I}_0' - z^2\mathcal{I}_0 = 0$ and $K_0(z)$ too. Since we have just shown that everywhere $\partial_t G_{\mathrm{H}} = G_\delta$ and G_δ given by (1.3) has the correct limiting behavior on the east-west axis, our expression for G_{H} (1.4) reduces there to (2.4a) and (2.4b). This has been verified independently with a Taylor series expansion of G_{H} about $\theta = 0$ and $\theta = \pm\pi$.

4. Properties of the Green's functions

In the integral expressions (2.1) and (2.5a) for G_δ and (2.2) and (2.5b) for G_{H}, the arguments of the integrands contain the similarity variable βtr. Our new expressions for G_δ (1.3) and for G_{H} (1.4) also contain this variable via the complex conjugate variables $z_\pm$ defined in (1.5). If time t and distance r were dimensional, the combination βtr is a non-dimensional variable. The mathematical problem has however already been formulated with non-dimensional time t and r or $\{x, y\}$ through scaling with some time scale T and length scale L, i.e. in (1.2a,b) the variables are actually non-dimensional $\tilde{t} = t/T$ and $\{\tilde{x}, \tilde{y}\} = \{x/L, y/L\}$ and non-dimensionally $\tilde{\beta} = \beta \times TL$. For convenience we have however dropped the tildes. In the graphs below we shall plot the response against non-dimensional $\{x, y\}$ and time t scaled with arbitrary L and T but in the numerical evaluations we have set $\beta = 1$.

4.1. *Response to impulsive forcing: G_δ*

Graphing the exact solution G_δ given in (1.3) is easy with available numerical packages although some care is required on the western axis where $\theta = \pm\pi$. Due to ambiguity as to how the Bessel functions behave as their arguments become purely imaginary ($z_\pm = \pm\mathrm{i}\sqrt{\beta tr}$), it is best to use a numerical grid that has no points exactly on the

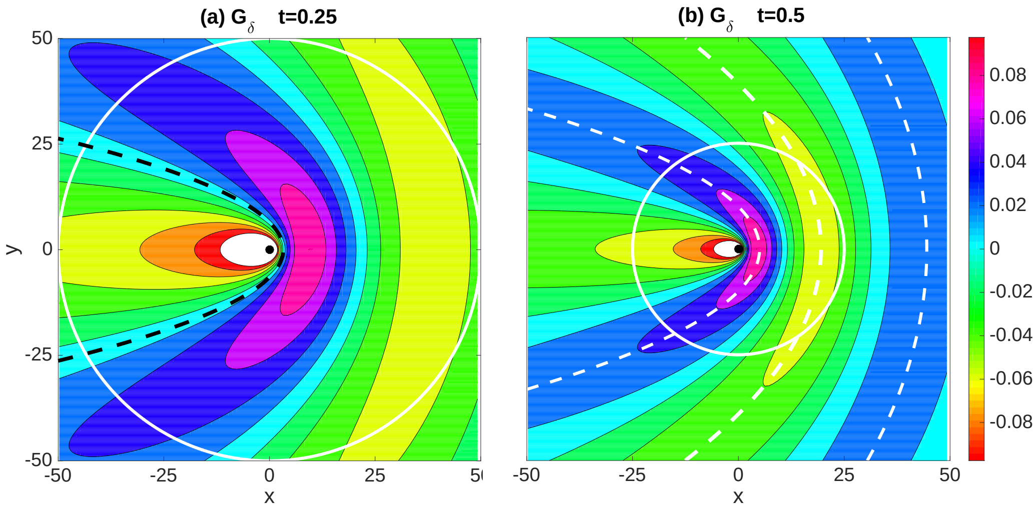

FIGURE 3. Contours of G_δ (1.3) at (a) non-dimensional time $t = 0.25$ and (b) $t = 0.5$. White circle in panel (a) has a radius $r = 50$ and in (b) a radius $r = 25$. Because of self-similarity in panel (b) at the double the time compared to panel (a), the pattern within the circle is exactly the same. Black dot • at the center $r = 0$ indicates the source origin. White space thereabouts indicates extreme negative values associated with the logarithmic singularity of G_δ (see text). In panel (a) the black dashed line is the parabola $2a\zeta = \pi/2$ with $\zeta = \sqrt{x + r}$ and $a = \sqrt{\beta t/2}$. Along this contour $G_\delta = 0$. In panel (b) the white dashed parabolas are $2a\zeta = (n + 1)\pi$ with $n = 0, 1, 2$.

western axis. Since spatially the response depends only on the similarity coordinates βtx, βty or βtr and θ, for any $t = t_0 > 0$ all information is contained in the response at t_0. But it is illuminating to graph the response as a function of time. As mentioned in the introduction, very little effort is required to create a movie that vividly illustrates the evolution.

Thus in figure 3 we chose non-dimensional time $t = t_0 = 0.25$ (panel (a)) and $t = 2t_0 = 0.5$ (panel (b)). In panel (a) we have drawn a circle with radius $r_0 = 50$ and in panel (b) with radius $r = \frac{1}{2}r_0 = 25$. Therefore in both panels the circles have $tr = t_0 r_0$ and the self-similarity is evident: in figure 3b the same pattern is seen within the circle as in figure 3a but shrunk to half the scale. For increasing time more of the 'banana' shaped regions appear to propagate from the east towards the source location indicated by '•'. An ever larger number gets wrapped about the origin, with increasing curvature.

West of the source a wake-like region exists forever concentrated about the western axis. In panel (a) the boundary of the wake is indicated by the dashed curve along which $G_\delta = 0$. Within this region, all streamlines indicate flow with the same sense of circulation about the origin but elongated in the western direction. East of the source, contours near the east-west axis are nearly north-south thus indicating predominantly north-south motions with velocity v advecting planetary vorticity. In the white area in figure 3 near the source location, the response exceeds some arbitrarily chosen (negative) amplitude threshold. Veronis (1958) was already able to sketch these patterns by numerically solving a partial differential equation similar to (2.11b) (see also Longuet-Higgins (1965)). Near the source location (the white region in figure 3), according to (3.15) the singular behavior persists.

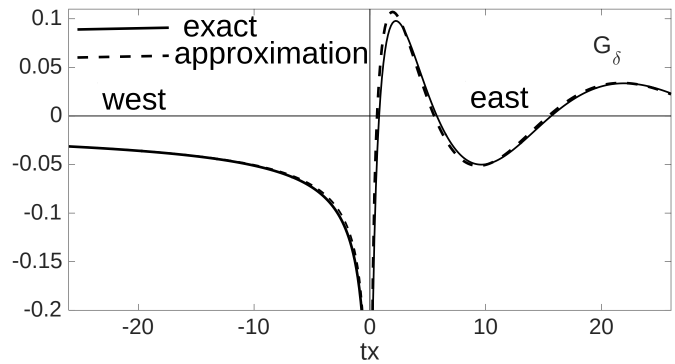

FIGURE 4. Graph showing the exact G_δ (1.3) on the east-west axis through the source and the approximation $G_\delta^{\rm a}$ (4.4*a,b*). According to (2.3*a*) to the east: $G_\delta = J_0(\rho)Y_0(\rho)/2$ and to the west according to (2.3*b*) $G_\delta = -I_0(\rho)K_0(\rho)/\pi$ with $\rho = \sqrt{\beta t|x|}$. For convenience we used $\beta = 1$.

With the known properties

$$z \to \infty: \; J_\nu(z) \sim \sqrt{2/(\pi z)}\cos\!\left(z-\tfrac{1}{2}\nu\pi-\tfrac{1}{4}\pi\right), Y_\nu(z) \sim \sqrt{2/(\pi z)}\sin\!\left(z-\tfrac{1}{2}\nu\pi-\tfrac{1}{4}\pi\right), \quad (4.1)$$

according to (1.3)

$$\beta tr \to \infty: \; G_\delta \sim -\frac{\cos(z_+ + z_-)}{2\pi\sqrt{z_+ z_-}}. \quad (4.2)$$

With the definitions of $z_\pm$ in (3.7) and the parabolic coordinates $\{\zeta, \eta\}$ in (3.8):

$$\beta tr \to \infty: \; G_\delta \sim -\frac{\cos(2a\zeta)}{2\pi\sqrt{a^2(\zeta^2+\eta^2)}} = -\frac{\cos(\sqrt{2\beta t(x+r)})}{2\pi\sqrt{\beta tr}} \equiv G_\delta^{\rm a}. \quad (4.3)$$

Lines of constant $\zeta = \sqrt{x+r}$ are parabolas that open towards the west ($x < 0$) as shown in figure 2. Some of these parabolas have been drawn in figure 3 as dashed curves. Longuet-Higgins (1965) already predicted that lines of constant phase would be such parabolas. The approximation $G_\delta^{\rm a}$ in (4.3) was recently found by Webb *et al.* (2016), but as the large-time behavior implied by an (inverse Laplace transform) integral representation of G_δ.

The approximation (4.3) predicts zeros for $2a\zeta = (n+\frac{1}{2})\pi$ ($n = 0, 1, \cdots$). The first zero ($n = 0$) has $2a\zeta = \pi/2$ which has been drawn in figure 3a as the dashed black parabola, delineating the 'wake'. The approximation predicts on the eastern side maxima/minima for $2a\zeta = (n+1)\pi$. For $n = 0, 1, 2$ these are the three white dashed parabolas drawn in figure 3b. It is seen that they form the 'spine' of the curved patterns.

The approximation reveals the salient behavior for large βtr that is hidden in the exact but complex expression (1.3) for G_δ. For large βtr or $\beta t|x|$ on the east-west axis

$$\theta = 0\,(\text{east}): \; G_\delta^{\rm a} = -\frac{\cos(2\sqrt{\beta tr})}{2\pi\sqrt{\beta tr}}, \quad \theta = \pm\pi\,(\text{west}): \; G_\delta^{\rm a} = -\frac{1}{2\pi\sqrt{\beta tr}}. \quad (4.4a,b)$$

In figure 4 we compare the approximation on this axis with the known exact solution(s) (2.3*a*,2.3*b*). This cross-section along the axis illustrates some of the features seen in figure 3. In particular, the first zero crossing with $2a\zeta = 2\sqrt{\beta tx} = \frac{1}{2}\pi$ on the eastern side corresponds to the 'wake' defined by $G_\delta = 0$ (the black parabola in figure 3a).

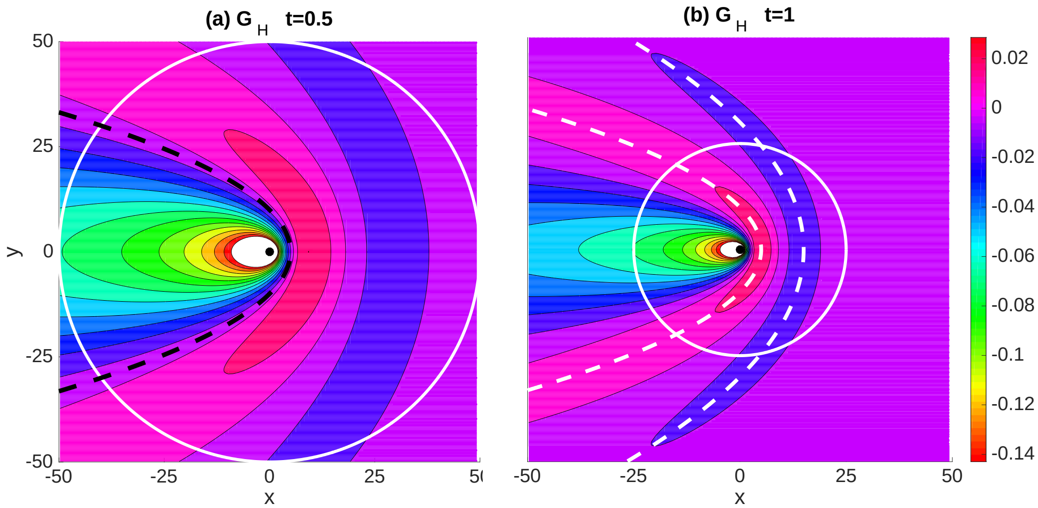

FIGURE 5. Contours of $G_{\rm H}$ at (a) non-dimensional time $t = 0.5$ and (b) $t = 1.0$. White circle in panel (a) has a radius $r = 50$ and in (b) a radius $r = 25$. In panel (a) the black dashed line line is the parabola $2a\zeta = \pi$ with $\zeta = \sqrt{x + r}$ and $a = \sqrt{\beta t/2}$. Along this curve $G_{\rm H} = 0$. In panel (b) the white dashed lines are for $2a\zeta = (n + 3/2)\pi$ with $n = 0, 1$.

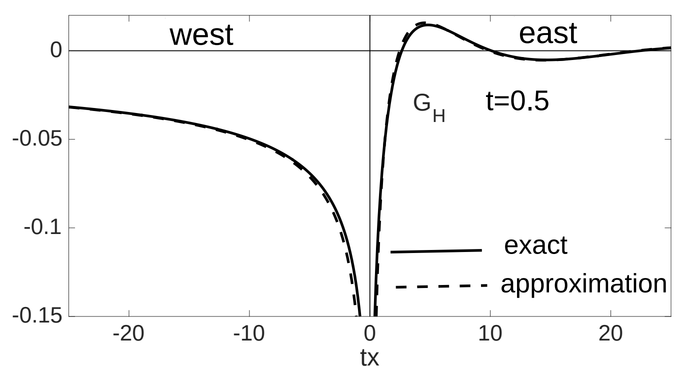

FIGURE 6. Graph showing the exact $G_{\rm H}$ (1.4) on the east-west axis through the source and the approximation $G^{\rm a}_{\rm H}$ (4.8a,b) at non-dimensional time $t = 0.5$. According to (2.4a) to the east: $G_{\rm H} = t[J_0(\rho)Y_0(\rho) + J_1(\rho)Y_1(\rho)]/2$ and to the west according to (2.4b) $G_{\rm H} = -t[I_0(\rho)K_0(\rho) + I_1(\rho)K_1(\rho)]/\pi$ with argument $\rho = \sqrt{\beta t|x|}$.

4.2. *Response to sustained forcing:* $G_{\rm H}$

In figure 5 we show contours of the exact solution $G_{\rm H}$ given in (1.4) for non-dimensional times $t = t_0 = 0.5$ (panel (a)) and $t = 2t_0 = 1$. As in figure 3 for G_δ, we have drawn in panel (a) a circle with radius $r_0 = 50$ and in panel (b) with radius $r = \frac{1}{2}r_0 = 25$. In both panels the circles have $tr = t_0r_0$ and spatial self-similarity is evident. The source location is again indicated by '•'. Close to the source according to (3.20) with increasing time the singularity grows in amplitude, if this can be said with regard to something that has infinite amplitude. Within the white areas in figure 5, $G_{\rm H}$ exceeds some (negative) amplitude threshold associated with this singularity.

According to (4.1), for large arguments $|z_\pm| \gg 1$, the terms within square brackets in

(1.4) become

$$
\begin{aligned}
z_+[J_1(z_+)Y_0(z_-)+J_0(z_-)Y_1(z_+)] &\sim -\frac{2}{\pi}\frac{z_+}{\sqrt{z_+z_-}}\sin(z_++z_-),\\
z_-[J_1(z_-)Y_0(z_+)+J_0(z_+)Y_1(z_-)] &\sim -\frac{2}{\pi}\frac{z_-}{\sqrt{z_+z_-}}\sin(z_++z_-).
\end{aligned}
\tag{4.5}
$$

Putting (4.5) in (1.4) yields

$$
\beta tr\to\infty:\quad G_{\rm H}\sim -\frac{1}{\pi}\frac{t\sin(z_++z_-)}{(z_++z_-)\sqrt{z_+z_-}}
\tag{4.6}
$$

and with (3.7), (3.8)

$$
\beta tr\to\infty:\quad G_{\rm H}\sim -\frac{1}{\pi}\frac{\sin(2a\zeta)}{\beta\zeta\sqrt{\zeta^2+\eta^2}} = -\frac{\sin(\sqrt{2\beta t(x+r)})}{\pi\beta\sqrt{x+r}\sqrt{2r}} \equiv G_{\rm H}^{\rm a}.
\tag{4.7}
$$

This agrees with the result of Kamenkovich (1989) who derived large time expansions of $G_{\rm H}$ via a consideration of the asymptotic properties of inverse Laplace transforms. There is a noticeable difference between G_δ and $G_{\rm H}$: whereas according to (4.3) amplitudes of G_δ decay with time as $t^{-1/2}$, amplitudes of $G_{\rm H}$ are constant (with the exception of the west-axis; see below). Nonetheless $G_\delta=\partial G_{\rm H}/\partial t$ and one easily verifies with (4.3) and (4.7) that also $G_\delta^{\rm a}=\partial G_{\rm H}^{\rm a}/\partial t$.

The approximation (4.7) predicts zeros for $2a\zeta=(n+1)\pi$ $(n=0,1,\cdots)$ and again $\zeta=\sqrt{x+r}$ and $a=\sqrt{\beta t/2}$. The first zero has $2a\zeta=\pi$ and the 'wake' defined by this curve on which $G_{\rm H}=0$ is the black dashed line in figure 5a. The approximation predicts on the eastern side maxima/minima for $2a\zeta=(n+\frac{3}{2})\pi$. The first two $(n=0,1)$ are the dashed parabolas drawn in figure 5b.

Comparison of figure 5 with figure 3 reveals a difference: in figure 5 the response to the east of the forcing appears to contain fewer of the typical patterns. Why this is can be illustrated with the far field approximation of $G_{\rm H}$ given by (4.7), i.e. for large βtr on the east-west axis:

$$
\theta=0\,(\text{east}):\; G_{\rm H}^{\rm a}=-\frac{\sin(2\sqrt{\beta tr})}{2\pi\beta r},\quad \theta=\pm\pi\,(\text{west}):\; G_{\rm H}^{\rm a}=-\frac{1}{\pi}\sqrt{\frac{t}{\beta r}}.
\tag{4.8a,b}
$$

In figure 6 we compare the approximation on the entire axis with the exact solution(s) (2.4a,2.4b). This explains why in figure 5 there are fewer of the parabolically-shaped regions visible east of the forcing: on the eastern axis for fixed time (4.4a) reveals that $G_\delta\propto 1/\sqrt{r}$ whereas (4.8a) indicates $G_{\rm H}\propto 1/r$, i.e. $G_{\rm H}$ decays more rapidly towards the east than G_δ with distance r from the source location. The two prominent patterns east of the source seen in figure 5a correspond to the first maximum and minimum in the cross section shown in figure 6, i.e. $2a\zeta=2\sqrt{\beta tx}=(n+\frac{3}{2})\pi$ and $n=0,1$. Finally, note that (4.6) shows that amplitudes do not decay nor grow with time t except exactly on the west-axis ($\zeta=0$) where

$$
\zeta\downarrow 0:\quad \frac{\sin(2a\zeta)}{\zeta}\to 2a=\sqrt{2\beta t}
\tag{4.9}
$$

and this singular limit leads to the unbounded growth of $G_{\rm H}$ displayed in (4.8b).

4.3. *Kinetic energy distributions*

The approximation (4.3) suggests that at a fixed location with increasing time, the quasi-wave field associated with G_δ disappears with $1/\sqrt{t}$. Thus, nothing but the singularity

(3.15) would remain. But a more relevant quantity is kinetic energy E. This is determined by gradients of the stream function $\psi = G_\delta$ and because with increasing time the spatial scales decrease, gradients increase. This compensates for the overall decrease of the amplitude of G_δ.

The kinetic energy associated with the Green's function is $E = \frac{1}{2}\boldsymbol{\nabla}G\boldsymbol{\cdot}\boldsymbol{\nabla}G$. The easiest way to calculate E is to use the fact that in parabolic coordinates

$$\boldsymbol{\nabla} = \frac{1}{\sqrt{\zeta^2+\eta^2}}\left[\hat{\boldsymbol{\zeta}}\frac{\partial}{\partial\zeta} + \hat{\boldsymbol{\eta}}\frac{\partial}{\partial\eta}\right] \tag{4.10}$$

with $\{\hat{\boldsymbol{\zeta}}, \hat{\boldsymbol{\eta}}\}$ the orthogonal unit vectors associated with $\{\zeta, \eta\}$ (see Morse & Feshbach (1953), Moon & Spencer (1961)). Without going into any further details, we find

$$\begin{aligned} E &= \frac{1}{2(\zeta^2+\eta^2)}\left[\left(\frac{\partial G}{\partial\zeta}\right)^2 + \left(\frac{\partial G}{\partial\eta}\right)^2\right] \\ &= \left(\frac{1}{4}\right)^2 \frac{\beta t}{\zeta^2+\eta^2}\left|J_0(z_+)Y_1(z_-) + J_1(z_-)Y_0(z_+)\right|^2 = E_\delta \end{aligned} \tag{4.11}$$

when $G = G_\delta$ given by (1.3) is substituted in (4.11). This may give the impression that the kinetic energy grows with time t. But, for large βtr it follows with (4.1) that

$$\beta tr \to \infty: \quad J_0(z_+)Y_1(z_-) + J_1(z_-)Y_0(z_+) \sim -\frac{2}{\pi}\frac{\sin(z_+ + z_-)}{\sqrt{z_+ z_-}}. \tag{4.12}$$

Squaring (4.12) and substitution in (4.11) yields for large βtr the approximation

$$E_\delta \sim \frac{1}{2}\frac{\sin^2(2a\zeta)}{\pi^2(\zeta^2+\eta^2)^2} = \frac{1}{2}\frac{\sin^2(\sqrt{2\beta t(x+r)})}{(2\pi r)^2} \equiv E_\delta^{\mathrm{a}}. \tag{4.13}$$

In figure 7 we show contours of kinetic energy E_δ (4.11). The patterns are similar to that of G_δ shown in figure 3. The one-term approximation (4.13) predicts maximal energy along parabolas $2a\zeta = (n + \frac{1}{2})\pi$ with $n = 0, 1, \cdots$ ($\zeta = \sqrt{x+r}$, $a = \sqrt{\beta t/2}$). In figure 7 the innermost dashed parabola is for $n = 0$ and coincides with the wake boundary shown in figure 3a. This is a location of maximal kinetic energy. In figure 7 the second parabola ($n = 1$) is seen to match the next pattern of maximal energy well. In figure 7 we have drawn a circle with radius $r = 40$. Going around this circle of radius $r = 40$ the peaks of energy are shown in figure 8 as well as for a circle of smaller radius $r = 30$. The approximation (4.13), based on the assumption $\beta tr \gg 1$, shows that at large r all maxima will have the same amplitude, as observed in figure 8. In polar coordinates the approximation

$$E_\delta^{\mathrm{a}} = \frac{1}{2}\frac{\sin^2(2a\zeta)}{(2\pi r)^2}, \qquad 2a\zeta = \sqrt{2\beta tr}\sqrt{1+\cos\theta} \tag{4.14}$$

shows that the energy peaks decay with distance $1/r^2$ from the source and the peak positions in terms of the polar angle θ are determined by $2\beta tr(1+\cos\theta) = (n+\frac{1}{2})^2\pi^2$. At fixed radius r with increasing time t more peaks appear as continuously more of the parabolic patterns seen in figure 3 coming from the eastern side get wrapped about the forcing origin.

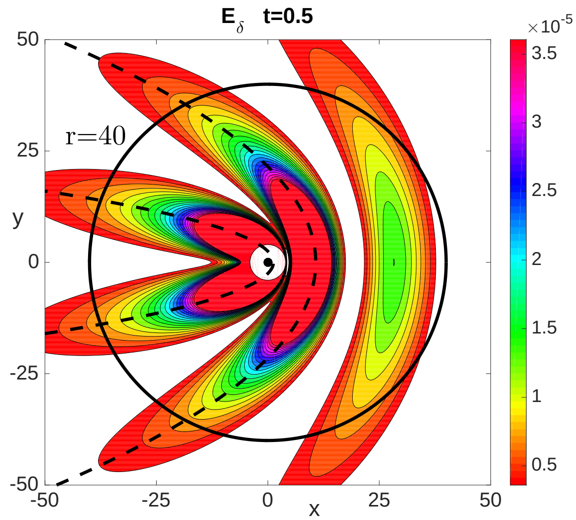

FIGURE 7. Contours of kinetic energy E_δ given by (4.11) at $t = 0.5$. The innermost dashed parabola is defined by $2a\zeta = (n + 1/2)\pi$ with $n = 0$ and $\zeta = \sqrt{x+r}$, $a = \sqrt{\beta t/2}$. This corresponds to the 'wake' boundary shown in figure 3a along which $G_\delta = 0$. The second parabola is for $n = 1$. Energy along the circle with radius $r = 40$ is shown in figure 8.

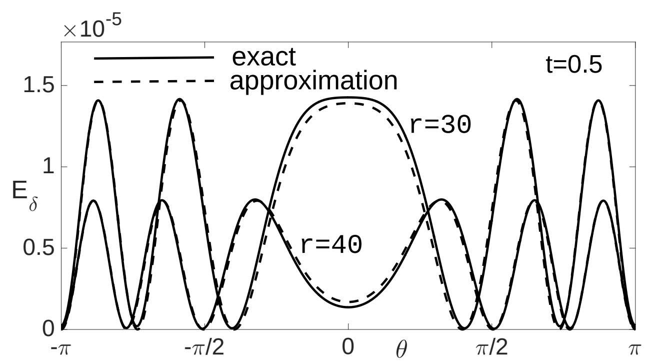

FIGURE 8. Kinetic energy E_δ (4.11) and the approximation E_δ^{a} (4.13) along circles of radius $r = 30$ and $r = 40$ at $t = 0.5$. The circle $r = 40$ is shown in figure 7.

The energy associated with G_{H} can be calculated exactly too and we find

$$\frac{\partial G_{\mathrm{H}}}{\partial \eta} = \frac{1}{\eta}\left\{t\left(G_\delta + \tfrac{1}{4}\left[J_1(z_+)Y_1(z_-) + c.c.\right]\right) - G_{\mathrm{H}}\right\}, \tag{4.15a}$$

$$\frac{\partial G_{\mathrm{H}}}{\partial \zeta} = \frac{1}{\zeta}\left\{t\left(G_\delta - \tfrac{1}{4}\left[J_1(z_+)Y_1(z_-) + c.c.\right]\right) - G_{\mathrm{H}}\right\} \tag{4.15b}$$

with G_δ as in (1.3) and G_{H} again given by (1.4). Division by η in (4.15a) may be cause of concern at first sight, but $\eta = 0$ corresponds to the east-axis and there according to (2.3a) and (2.4a):

$$\begin{aligned} \eta = 0 \ (\text{east}): G_\delta = \tfrac{1}{2}J_0(\rho)Y_0(\rho), \quad G_{\mathrm{H}} = \tfrac{1}{2}t\left[J_0(\rho)Y_0(\rho) + J_1(\rho)Y_1(\rho)\right], \\ \text{and} \quad \tfrac{1}{4}\left[J_1(z_+)Y_1(z_-) + c.c.\right] = \tfrac{1}{2}J_1(\rho)Y_1(\rho), \quad \rho = \sqrt{\beta t r} \end{aligned} \tag{4.16}$$

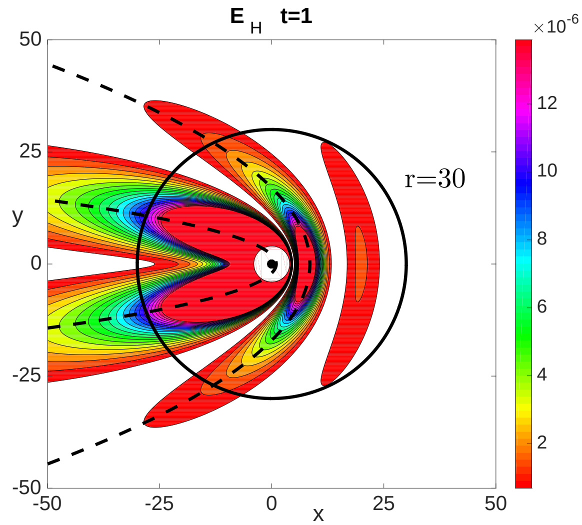

FIGURE 9. Contours of energy E_{H} according to (4.18) at $t=1$. The innermost dashed parabola is for $2a\zeta=\sqrt{2}$ with $\zeta=\sqrt{x+r}$, $a=\sqrt{\beta t/2}$. This lies inside to the 'wake' boundary shown in figure 5a along which $G_{\mathrm{H}}=0$ and for which $2a\zeta=\pi$. Energy along the circle with radius $r=30$ is shown in figure 10.

so that in the limit $\eta=0$ the numerator of (4.15a) vanishes and an expansion in small η can be shown to give a finite answer for $\partial G_{\mathrm{H}}/\partial\eta$. Also the limit $\zeta=0$ appears dangerous in (4.15b) but again a finite answer is obtained by taking into account that there

$$\begin{aligned}\zeta=0\ (\text{west}):\quad G_\delta=-\frac{I_0(\rho)K_0(\rho)}{\pi},\quad G_{\mathrm{H}}=-\frac{t}{\pi}\left[I_0(\rho)K_0(\rho)+I_1(\rho)K_1(\rho)\right],\\ \tfrac{1}{4}[J_1(z_+)Y_1(z_-)+c.c.]=\frac{I_1(\rho)K_1(\rho)}{\pi},\quad \rho=\sqrt{\beta t r}.\end{aligned}\tag{4.17}$$

Therefore in the limit $\zeta=0$ the numerator of (4.15b) vanishes and $\partial G_{\mathrm{H}}/\partial\zeta$ is well-defined. Contours of

$$E_{\mathrm{H}}=\frac{1}{2(\zeta^2+\eta^2)}\left[\left(\frac{\partial G_{\mathrm{H}}}{\partial\zeta}\right)^2+\left(\frac{\partial G_{\mathrm{H}}}{\partial\eta}\right)^2\right]\tag{4.18}$$

are shown in figure 9. The energy along the circle with radius $r=30$ drawn in figure 9 is shown in figure 10.

Whereas it is easy to find the approximation (4.13) for the kinetic energy E_δ by employing the asymptotic properties of J_ν, Y_ν according to (4.1), things become quite difficult if the same route is taken here for E_{H}: it requires the rarely used higher-order corrections to (4.1). Instead we calculate the approximation by differentiation of (4.7). This yields in polar coordinates

$$\begin{aligned}E_{\mathrm{H}}\sim\frac{1}{2}\frac{1}{(2\pi r)^2}\left(\frac{t}{\beta r}\right)\frac{1}{1+\cos\theta}\left[2\cos^2(2a\zeta)-\frac{2(3+\cos\theta)\cos(2a\zeta)\sin(2a\zeta)}{(2a\zeta)}\right.\\ \left.+\frac{(5+3\cos\theta)\sin^2(2a\zeta)}{(2a\zeta)^2}\right]\equiv E_{\mathrm{H}}^{\mathrm{a}},\qquad 2a\zeta=\sqrt{2\beta t}\sqrt{r(1+\cos\theta)}.\end{aligned}\tag{4.19}$$

For large time the first term within square brackets, $\cos^2(2a\zeta)$, dominates but the next two terms cannot be discarded: they are both required to negate the singular behavior

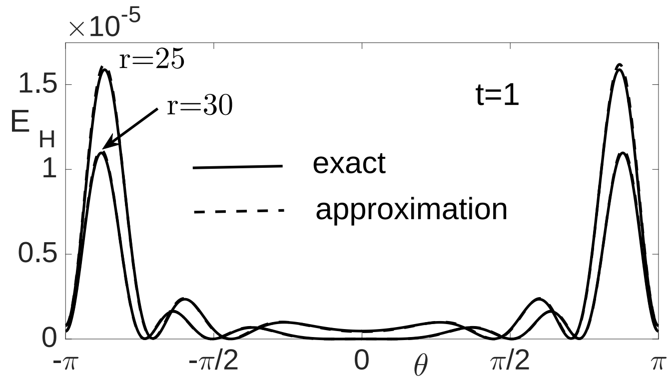

FIGURE 10. Contours of kinetic energy E_{H} (4.18) at $t = 1$ and the approximation $E_{\mathrm{H}}^{\mathrm{a}}$ (4.19) along circles of radius $r = 25$ and $r = 30$ at $t = 1$. The circle $r = 30$ is shown in figure 9.

of the prefactor $1/r(1 + \cos\theta) = 1/\zeta^2$. In other words, in the limit $\theta = \pm\pi$ or $\zeta = 0$ (the western axis) all three terms are required. In that limit $\sin(2a\zeta)/(2a\zeta) \to 1$ and the bracketed term in (4.19) evaluates to

$$[2 - 2(3 - 1) + (5 - 3)] = 0$$

and expansions of the second and third term in powers of small ζ always yield a finite result. In figure 10 we compare the appxomation (4.19) with the exact energy along the circle of radius $r = 30$ also shown in figure 9 and at a smaller radius $r = 25$. We simply chose $t = 1$ which was also used for figure 5b. Comparison of figures (9) and (10) with the corresponding figures (7) and (8) for G_δ reveals that for G_{H} the kinetic energy is dominated by two plumes on the western side of the forcing. Another differences is that (4.19) shows that away from the western axis, E_{H} decays with distance from the forcing with $1/r^3$ while linearly growing in time while (4.13) shows that E_δ decays with $1/r^2$ with amplitudes that are independent of time.

Finally, as in figure 7 for E_δ we have drawn in figure 9 two parabolas $\zeta =$ constant that fit the maximal energy patterns. For G_δ in figure 7 the innermost parabola coincided with the wake boundary $G_\delta = 0$ and $2a\zeta = \frac{1}{2}\pi$: this is the first maximum of the leading-order term $\sin^2(2a\zeta)$ in (4.14). But for E_{H} the first maximum is not determined by $\cos^2(2a\zeta)$ with maxima at $2a\zeta = (n + 1)\pi$ but by the combination of all three terms within the square brackets in (4.19). We find that the parabolic axis through the dominant energy pattern in figure 9 lies well within the wake region: in figure 5a the wake boundary (dashed parabola) is defined by $2a\zeta = \pi$ but in figure 9 the axis was found to coincide with $2a\zeta = \sqrt{2} < \pi$ and the second parabola with $2a\zeta = 4 < 2\pi$. At later times (not shown) the tendency is that the axis of the dominant energy 'plumes' of E_{H} moves further towards the west-axis, i.e. further into the interior of the wake region.

5. Discussion

In this paper we have shown that two-dimensional Green's functions G_δ and G_{H} given by (1.3) and (1.4), respectively, solve the forced Rossby wave equation (1.2). Previously only known via integral representations, these new compact expressions provide a complete description of the response. They reduce on the east-west axis to the long-known exact expressions discussed in §2, i.e. ($2.3a, 2.3b$) for G_δ and ($2.4a, 2.4b$) for G_{H} and far from the forcing location to the asymptotic forms (4.3) and (4.7), respectively. The latter were also known via transform methods but here they arise directly from the properties of the Bessel functions $J_n(z), Y_n(z)$ for large (complex) arguments z.

Exact explicit expressions for Green's functions were known in one-dimensional (Cahn (1945); Rossby (1945)) and three-dimensional (Dickinson (1969*a*,*b*)) settings only. Usually solutions of the forced problem are sought through transform methods (see Veronis (1958); Longuet-Higgins (1965); Kamenkovich (1989); Llewellyn-Smith (1997) but also the recent studies by McKenzie (2014); Webb *et al.* (2016)). In two-dimensional problems this has led to integral representations like those mentioned in §2.

A crucial development has been that the integral representation for G_δ can be written as (3.1). From this the closed-form expression (1.3) for G_δ followed via the work of Dixon & Ferrar (1933) as discussed in §3. The validity of this solution has been verified in §3.1 and in §3.2 we derived and verified the expression (1.4) for G_{H}. This becomes very efficient through the introduction of the complex conjugate variables $z_\star = \zeta + \mathrm{i}\eta$, $\bar{z}_\star = \zeta - \mathrm{i}\eta$ defined in (3.7). In particular, the Rossby wave operator then assumes the symmetric form given in (3.11). That contour patterns of G_δ and G_{H} shown in §4 in figure 3 and figure 5 coincide largely with the parabolas $\zeta = \sqrt{r+x} =$ constant is perhaps not surprising since if on the right-hand side of (1.2a) instead of $\delta(t)$ periodic forcing $\exp(\mathrm{i}\omega t)$ is assumed, lines of constant phase are also $\zeta =$ constant (see Rhines (2003)).

The parabolic coordinates $\{\zeta, \eta\}$ are of wider interest in the context of non-divergent Rossby waves. First note that the form of $\mathcal{L}$ in (3.10) suggests that there is no real distinction between ζ and η whereas in the Cartesian $\{x, y\}$ formulation longitude x introduces an 'asymmetry' not obvious in (3.10) except for the sign-difference between the ζ and η terms multiplying β (the same spatial part of this Rossby wave operator for a steady, frictional version of the vorticity equation was previously considered in ocean circulation context in Maas (1989); Zimmerman & Maas (1989) and Boyd & Sanjaya (2014)). Let us further note that in as much that the Green's functions are stream functions ψ with the associated velocity components $u = -\partial_y\psi, v = \partial_x\psi$, equation ($2.11b$) is simply

$$\partial_t(xu + yv) + \tfrac{1}{2}\beta y\,\psi = 0 \quad \text{with} \quad xu + vy = \mathbf{u}\cdot\mathbf{r}, \quad \mathbf{u} = u\mathbf{i} + v\mathbf{j},\, \mathbf{r} = x\mathbf{i} + y\mathbf{j} \tag{5.1}$$

and $\{\mathbf{i}, \mathbf{j}\}$ the customary unit vectors associated with $\{x, y\}$. The projection of the velocity vector $\mathbf{u}$ on the position vector $\mathbf{r}$ is $\mathbf{u}\cdot\mathbf{r} = ru_r$ with u_r the radial velocity component in cylinder coordinates (see figure 1). In other words, in the wave field associated with the Green's functions the radial velocity component evolves according to $\partial_t r u_r + \frac{1}{2}\beta y\psi = 0$. It is not clear to us whether this has a physical meaning. However, leaving out a common factor $\frac{1}{2}$, in parabolic coordinates (5.1) becomes

$$\frac{\partial}{\partial t}\left(\eta\frac{\partial}{\partial\zeta} - \zeta\frac{\partial}{\partial\eta}\right)\psi + \beta\zeta\eta\psi = 0. \tag{5.2}$$

Further, differentiation of (5.1) with respect to x and multiplication of the Rossby wave equation by y allows for the elimination of the β-terms which results in

$$\partial_t\left\{y\nabla^2 + 2\partial_x\left(x\partial_y - y\partial_x\right)\right\}\psi = 0 \tag{5.3}$$

but in the parabolic coordinates (5.3) assumes the form

$$\frac{\partial}{\partial t}\left\{\frac{\partial^2}{\partial\zeta\partial\eta} + \frac{\eta}{\zeta^2+\eta^2}\frac{\partial}{\partial\zeta} + \frac{\zeta}{\zeta^2+\eta^2}\frac{\partial}{\partial\eta}\right\}\psi = 0. \tag{5.4}$$

Remarkably, integrating (5.4) in time shows that the Green's functions are determined by a *second-order* partial differential equation, which, moreover, is entirely symmetric in parabolic coordinates ζ, η. Additionally, the form of the Rossby wave operator $\mathcal{L}$ (3.10) in these coordinates suggests that the parabolic coordinates are rather 'natural' coordinates for non-divergent Rossby waves.

This raises the question why the response in the forced problem considered here is dominated by the westward parabolas $\zeta = \sqrt{r+x}$ while the opposite parabola $\eta = \sqrt{r-x}$ only plays a role in providing overall amplitude attenuation via inverse (fractional) powers of $r = \frac{1}{2}(\zeta^2 + \eta^2)$. This can be understood with the analyses of Longuet-Higgins (1965) and the more recent work by McKenzie (2014), i.e. via considerations of the dispersion relation for monochromatic waves, the group velocity and the method of stationary phase. But a cursory examination of the properties of $\mathcal{L}$ in parabolic coordinates, i.e. (3.10), indicates that free, parabolically-shaped Rossby waves following lines of constant $\eta = \sqrt{r-x}$ instead of $\zeta = \sqrt{r+x}$ do also exist at any given frequency. The repercussions of this observation are left for a future study.

A few final remarks are in order: The singular behavior found for G_δ in (3.15) and G_{H} in (3.20) at the forcing location persists. For G_{H} this is not surprising since the forcing is maintained but for G_δ this is counterintuitive since one can interpret G_δ for some $t = t_0 > 0$ as a given initial stream function $\psi_0(x,y) = \psi(x,y,t_0)$. This initial condition for $t = t_0$ can be developed in plane Rossby waves with the spectrum $A_0(k,l)$ and for $t > t_0$ the field would evolve as

$$\psi(x,y,t) = \iint A_0(k,l)\mathrm{e}^{\mathrm{i}(\omega t - kx - ly)}\mathrm{d}k\mathrm{d}l$$

with ω satisfying the well-known dispersion relation

$$\omega = -\frac{\beta k}{k^2 + l^2}.$$

Without explicitly knowing the spectrum $A_0(k,l)$, one would think that dispersion leads to the disappearance of the singularity. But it does not. The 'shrinking' of the patterns via the similarity variable βtr towards the origin is also baffling although one might see this as a confirmation of the long-known properties of the Rossby waves: short waves (small spatial scales) have small group velocities (Pedlosky (1987)).

The Rossby wave equation describes the time-evolution of vorticity q which for the Green's functions is $q = \nabla^2 G$. This can be calculated quickly. For example, with the variables $\{z_\star, \bar{z}_\star\}$, introduced in (3.7),

$$\nabla^2 = \frac{4}{z_\star \bar{z}_\star}\frac{\partial^2}{\partial z_\star \partial \bar{z}_\star} \quad \text{and} \quad q_\delta \equiv \nabla^2 G_\delta = \frac{\beta t}{4r}[J_1(z_+)Y_1(z_-) + J_1(z_-)Y_1(z_+)] \tag{5.5}$$

after substitution of (1.3) and using $J_0' = -J_1$, $Y_0' = -Y_1$. For large arguments, i.e. far from the forcing, apart from a constant prefactor, q_δ behaves as $\cos(2a\zeta)/r^{3/2}$. The asymptotic energy distribution given in (4.14) behaves as $\sin^2(2a\zeta)/r^2$ and we thought that perhaps the 'empty' spaces seen in the energy distribution in figure 7 might be filled by $r \times \mathcal{E}_\delta$ with enstrophy $\mathcal{E}_\delta = \frac{1}{2}q_\delta^2$ so that a conservation law of the form $\partial_t(E_\delta + r\mathcal{E}_\delta) = 0$ would follow. This was nearly so, but not exactly. Thus we have no good understanding yet of the E_δ pattern seen in figure 7 nor of the energy distribution E_{H} in figure 9. A proper energy flux formulation is lacking in terms of recognizable physical quantities (see also Rhines (1975)). At best we can draw attention to the salient differences between E_δ and E_{H}: whereas figures 7 and 8 show that at any distance and given time t peaks of energy E_δ have equal amplitude and occur both west and east of the forcing, figures 9 and 10 show that the energy E_{H} associated with the sustained forcing is predominantly found west of the forcing. The peak amplitudes of E_δ do not vary with time t while with distance r from the source $E_\delta \propto 1/r^2$ (see (4.14)) but E_{H} grows with time t and decays more rapidly, i.e. $E_{\mathrm{H}} \propto 1/r^3$ (see (4.19)). The temporal behavior is not surprising in that continued forcing leads to growth in energy but the spatially more confined nature of E_{H} as compared to that of E_δ is surprising.

In as much in that the barotropic, non-divergent Rossby wave is a small but fundamental element in the realm of theoretical geophysical fluid dynamics, this study may stimulate interest beyond the current study to search for simple closed-form solutions of forced *divergent* Rossby waves (waves with finite Rossby deformation radius). This introduces finite group velocity for very long waves and more can then perhaps be said about the evolution of energy distributions and may help recognize 'where' wave energy goes. In view of our results there is reason to be optimistic that the complicated integral representation of Veronis (1958) for divergent Rossby waves and the elegant result of Webb *et al.* (2016) can be reduced to simpler expressions.

Another possible strategy is to consider a 'switch-on/switch-off' source, that is, the response G_δ which Veronis (1958) called a 'tweak', followed by an 'anti-tweak'. This will eliminate the singularity at the forcing location and energy will subsequently be finite everywhere. The simplicity of our expression for G_δ (1.3) allows for quick visualization of such a scenario and further mathematical analysis but this too is left for future research.

RCK acknowledges support from National Science Foundation grants OCE 10-32256 and OCE 15-38559. We thank two anonymous referees and Stefan Llewellyn-Smith for their insightful comments of the manuscript.

REFERENCES

Boyd, J.P. & Sanjaya, E. 2014 Geometrical effects of western intensification of wind-driven ocean currents: The stommel model, coastal orientation, and curvature. *Dynamics of Atmospheres and Oceans* **65**, 17–38.

Cahn, A. J. 1945 An investigation of the free oscillations of a simple current system. *J. Meteor.* **2** (2), 113–119.

Dickinson, R.E 1969*a* Propagators of atmospheric motions 1. excitation by point impulses. *Rev. Geophys.* **7** (3), 483–514.

Dickinson, R.E. 1969*b* Propagators of atmospheric motions 2. excitation by switch-on sources. *Rev. Geophys.* **7** (3), 515–538.

Dixon, A.L. & Ferrar, W.L. 1933 Integrals for the products of two bessel functions. *Quart. J. of Math.* **4**, 193–208.

Erdélyi, A., ed. 1953 *Higher transcendental functions*, *3*, vol. 2. McGraw-Hill.

Hough, S. S. 1898 On the application of harmonic analysis to the dynamical theory of the tides. - part ii. on the general integration of laplaces dynamical equations. *Phil. Trans (A)* **191**, 139–185.

Kamenkovich, V.M. 1989 Development of rossby waves generated by localized effects. *Oceanology* **29 (1)**, 1–11.

Llewellyn-Smith, S.G. 1997 The motion of a non-isolated vortex on the beta-plane. *J. Fluid Mech.* **346**, 149–179.

Longuet-Higgins, M.S. 1965 The response of a stratified ocean to stationary or moving wind-systems. *Deep-Sea Research* **12**, 923–973.

Maas, Leo RM 1989 A closed form green function describing diffusion in a strained flow field. *SIAM Journal on Applied Mathematics* **49** (5), 1359–1373.

Magnus, W., Oberhettinger, F. & Soni, R.P. 1966 *Formulas and theorems for the special functions of mathematical physics*, 3rd edn. Springer-Verlag.

MARGULES, M. 1893 Luftbewegungen in einer rotierenden sphäroidschale (ii. teil). *Sitz. der Math. - Naturwiss. Klasse, Kais. Akad. Wiss., Wien* **102**, 11–56.

MCKENZIE, J.F. 2014 The group velocity and radiation pattern of rossby waves. *Geophys. Astrophys. Fluid Dyn.* **108 (3)**, 258–268.

MOON, P. & SPENCER, D. E. 1961 *Field Theory Handbook*. Springer.

MORSE, P.M. & FESHBACH, H. 1953 *Methods of Theoretical Physics*. McGraw-Hill.

OLVER, F.W.J., LOZIER, D.W., BOISVERT, R.F. & CLARK, C.W., ed. 2010 *NIST Handbook of Mathematical Functions*. Cambridge University Press.

PEDLOSKY, J. 1987 *Geophysical Fluid Dynamics*, 2nd edn. New York, U.S.A.: Springer-Verlag.

RHINES, P.B. 1975 Waves and turbulence on a beta-plane. *J. Fluid. Mech.* **69**, 417–443.

RHINES, P.B. 2003 Rossby waves. In *Encyclopedia of Atmospheric Sciences* (ed. J.R Holton, J.A. Curry & J.A. Pyle), pp. 1–37. Academic Press: Oxford.

ROSSBY, C.-G 1945 On the propagation of frequencies and energy in certain types of oceanic and atmospheric waves. *J. Meteor.* **2** (4), 187–204.

ROSSBY, C.-G. & COLLABORATORS 1939 Relations between variations in the intensity of the zonal circulation of the atmosphere and the displacements of the semi-permanent centres of action. *J. Marine Res.* **2**, 38–54.

VERONIS, G. 1958 On the transient response of a beta-plane ocean. *J. Oceanogr. Soc. Japan* **14 (1)**, 1–5.

WEBB, G.M., DUBA, C.T. & HU, Q. 2016 Rossby wave green's functions in an azimuthal wind. *Geophys. Astrophys. Fluid Dyn.* **110 (3)**, 224–258.

ZIMMERMAN, JTF & MAAS, LRM 1989 Renormalized greens function for nonlinear circulation on the β plane. *Physical Review A* **39** (7), 3575.